Effect of laser post-processing on surface roughness of fused deposition modeling (FDM) part

S.N.H. Mazlan[1], M.R. Alkahari[1,2,*], F.R. Ramli[1,2], N.A. Maidin[3]

[1)]Faculty of Mechanical Engineering, Universiti Teknikal Malaysia Melaka, Hang Tuah Jaya, 76100 Durian Tunggal, Melaka, Malaysia
[2)]Centre of Advanced Research on Energy, Universiti Teknikal Malaysia Melaka, Hang Tuah Jaya, 76100 Durian Tunggal, Melaka, Malaysia
[3)]Faculty of Engineering Technology, Universiti Teknikal Malaysia Melaka, Hang Tuah Jaya, 76100 Durian Tunggal, Melaka, Malaysia

[*]Corresponding e-mail: rizalalkahari@utem.edu.my

Keywords: Fused deposition modeling (FDM); laser post-processing; surface roughness

ABSTRACT – Fused Deposition Modeling (FDM) is the common technique in Additive Manufacturing (AM) processes due to its numerous benefits. However, parts produced via FDM have poor surface quality compared to other AM processes. Thus, in this paper, laser post-processing is used to improve the surface finishing of the FDM part. After the part is printed, the surface is post-processed using CO_2 laser under various setting conditions. The effects of laser speed and laser power on the surface roughness are studied. The results show improvement in the surface roughness value after the laser beam applied on the specimen surfaces. This can be achieved through the control of laser speed and laser power.

1. INTRODUCTION

Additive manufacturing (AM) or 3D printing is a group of processes that produces 3D physical part layer by layer from computer aided design (CAD). There are many available processes being grouped under AM such as stereolithography, selective laser sintering (SLS), fused deposition modeling (FDM), direct laser metal sintering (DLMS) and 3D printing [1]. FDM is the most used in AM technique because it has an ability to produce the complex geometry part in a short building time, the machines are relatively easy to be handled and others. However, the ability of the FDM system and AM in general to produce an aesthetically appealing product with good mechanical properties such as dimensional accuracy and strength are still not comparable to other established processes [2].

Researchers have proposed methods to improve the surface roughness of the FDM printed parts. Rajendran et al stated the optimization of FDM is necessary to improve the quality of the part, especially on finishing [3]. Meanwhile, Mohamed et al reviewed that the methods to improve the surface finish by optimization of build orientation, layer thickness, fabrications parameter optimization and post-processing treatment [4]. Yasa studied on the improvement of surface finish for SLS technique by the approaching method of laser-re-melting. This method has successfully increased the mechanical properties in terms of porosity and surface roughness [5]. Therefore, in this paper, laser post-processing technique is used to improve the surface finishing of the FDM part, and the effect on the surface roughness is evaluated.

2. METHODOLOGY

The experiments were carried out using the Flashforge Creator Pro 3D printer for parts fabrication. Later, Trotec Laser (Speedy 300 Flexx) was used for the laser post-processing on the surface of the printed parts. The parts were fabricated using acrylonitrile butadiene styrene (ABS). The surface roughness of the printed parts was measured before and after the laser post-processing. In order to study the effect of the parameters on surface roughness, the specimens were post-processed at various laser speeds and power. The parts fabricated using FDM, and the setting of the laser are set as tabulated in Table 1 and Table 2 respectively.

Table 1 FDM parameter for 3D printed part fabrication

Parameter	Specification
Layer thickness (mm)	0.35
Infill density (%)	70
Raster angle (°)	45
Infill pattern	Line pattern

Table 2 Laser parameter setting

Parameter	Specification
Type	CO_2
Power (W)	10 to 70
Speed (mm/s)	50 to 110

3. RESULTS AND DISCUSSION

Figure 1 compares the surface roughness of 3D printed part when observed using an optical microscope before and after the post-processing. Figure 1(a) shows the line of the deposited filament which are well arranged and organized at raster angle of 45° during 3D printing. Whereas Figure 1(b) illustrates the surface of the same surface after being irradiated by the laser. By comparing these figures, it indicates that the cylindrical shape of the ABS filament becomes into small-sized agglomerate after being exposed to the laser irradiation. During post-processing, reheating of material occurs and turns it into a liquid form. The material then filled the spaces between the cylindrical shaped ABS. The continuous heating and cooling of the ABS material have caused the surface to be melted. As a result, a flatter surface was produced due to the flow of molten material which cover the gap between the spaces.

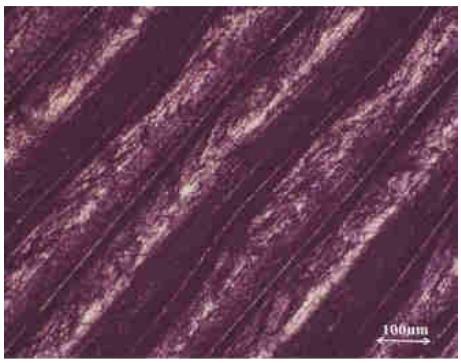

(a) Before post-processing

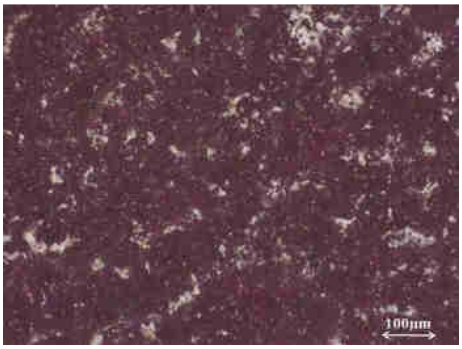

(b) After post-processing

Figure 1 FDM surface before and after post processing at a laser speed of 50 mm/s and power of 70 W

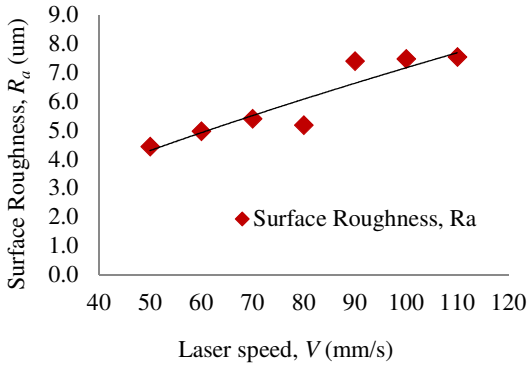

Figure 2 Effect of laser speed on surface roughness

Figure 2 indicates the effect of laser speed on the surface roughness as the speed was increased from 50 to 110 mm/s. Generally, it is found that by increasing laser speed during post-processing produces poorer surface roughness. At the high laser speed, the duration of laser irradiation on the printed surface is too short and does not affect the surface roughness.

On the other hand, Figure 3 shows the effect when the laser power is increased from 10 W to 70 W. It is found that the value of surface roughness is better at higher laser power. When the laser power is high, the energy density becomes more prominent and allows the temperature to increase and melt the material on the surface. As a result, the melted material able to flow due to the increase in its viscosity. Therefore, the material flows freely and fill in the gap between the deposited filament. However, the laser power is not recommended to be more than 70W because it may burn and affect the color of the 3D printed part. Nevertheless, increasing the laser power during post-processing is relatively effective in improving the surface roughness of the 3D printed part produced via FDM.

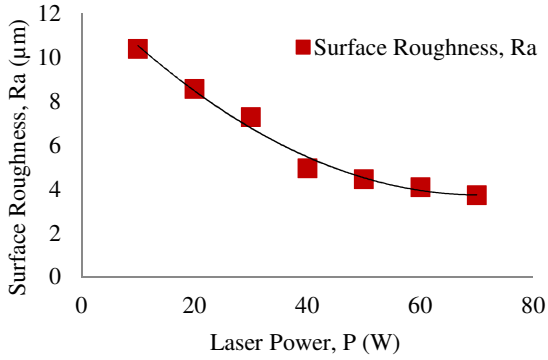

Figure 3 Effect of laser power on surface roughness

4. CONCLUSIONS

FDM is a potential additive manufacturing process to produce functional prototypes. In this study, laser post-processing was experimentally analyzed in order to enhance surface roughness of the FDM parts. It is found that, laser post-processing is a promising method to improve the roughness of FDM parts through the control of the laser speed and laser power.

ACKNOWLEDGEMENT

The authors would like to thank Universiti Teknikal Malaysia Melaka (UTeM) the support and Ministry of Education (MOE) for the research grant RAGS/1/2015/2015/TK0/FTK/03/B00113.

REFERENCES

[1] P. Jain and A. Kuthe, "Feasibility study of manufacturing using rapid prototyping: FDM approach," *Procedia Engineering*, vol. 63, pp. 4-11, 2013.

[2] H.A Habeeb, M.R. Alkahari, F.R. Ramli, R. Hasan and S. Maidin, "Strength and porosity of additively manufactured PLA using a low cost 3D printing," *Proceedings of Mechanical Engineering Research Day 2016*, 2016, pp 69-70.

[3] R. Anitha, S. Arunachalam and P. Radhakrishnan, "Critical parameters influencing the quality of prototypes in fused deposition modelling," *Journal of Materials Processing Technology*, vol. 118, no. 1-3, pp. 385-388, 2001.

[4] O. Mohamed, S. Masood and J. Bhowmik, "Optimization of fused deposition modeling process parameters: a review of current research and future prospects," *Advances in Manufacturing*, vol. 3, no. 1, pp. 42-53, 2015.

[5] E. Yasa and J. Kruth, "Microstructural investigation of selective laser melting 316L stainless steel parts exposed to laser re-melting," *Procedia Engineering*, vol. 19, pp. 389-395, 2011.

Tracking error compensation of XY table ball screw driven system using Cascade Fuzzy P+PI

Z. Retas[1,*], L. Abdullah[1], S.N. Sy Salim[2], Z. Jamaludin[1], N.A. Anang[1]

[1)]Faculty of Manufacturing Engineering Universiti Teknikal Malaysia Melaka, Hang Tuah Jaya, 76100 Durian Tunggal, Melaka, Malaysia
[2)]Faculty of Engineering Technology Universiti Teknikal Malaysia Melaka, Industrial Campus, Hang Tuah Jaya, 76100 Durian Tunggal, Melaka, Malaysia

[*]Corresponding e-mail: zain@pmm.edu.my

Keywords: XY Machine; Cascade P+PI; Fuzzy Control

ABSTRACT –This study describes the potential of the fuzzy logic technique and cascade controller in improving the tracking performance of the XY Table Ball Screw Driven System. The proposed controller used in this research is Cascade Fuzzy P+PI. This technique was compared with PI and Fuzzy-PI controller. The performances of the systems were analyzed in two cases, with and without disturbance. The results show that the combination of Fuzzy Logic technique with Cascade Controller, which is known as Cascade Fuzzy P+PI, successfully provide a good tracking performance with an increase of 56% compared to other methods tested in this research.

1. INTRODUCTION

Most controllers of the machine tool servo designs are still based on the well-known Proportional Integral Derivative, PID controller. This controller is considered as a generic controller that is widely used in industrial control system [1][2][3]. In this study, cutting force is considered as a disturbance. The method proposed is based on Cascade P+PI controller, which successfully contributed in increasing the quality of end products and productivity, due to the ability of the proposed method in saving the machining time[4]. The controllers were designed to cater different spindle speeds.

This paper deals with the Cascade Fuzzy P+PI method that is used to control the XY Table Ball Screw Driven System. This approach is an extension to the Conventional Cascade P+PI controller that is previously tested to the similar system as reported in [5]. The aim of this research is to improve the tracking performance of the XY Table Ball Screw Driven System.

This is performed by adding the fuzzy logic control algorithm that is used to tune the parameter of the generic controller at the outer, so that the tracking error can be reduced.

2. METHODOLOGY

In this study, an XY Table Ball Screw Driven System which is composed of an XY feed table of milling machine (Googol Tech GXYZ 202010 series). Figure 1 shows the experimental setup of the XY Table Ball Screw Driven System used in this study.

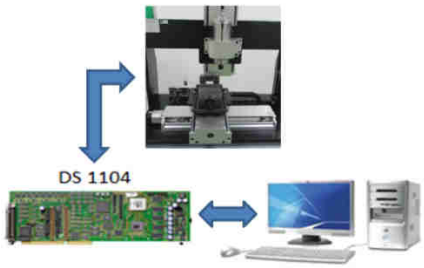

Figure 1 Experimental setup for XY Table Ball Screw Driven System feed table of milling machine

The proposed method used in this study is a combination between Cascade P+PI and Fuzzy control. Fuzzy logic controller is a knowledge driven method. In this study, fuzzy logic is that of a proportional gain, Kp, for the outer loop of the system the variations that occur on the output response. Figure 2 shows the structure of Cascade Fuzzy P+PI.

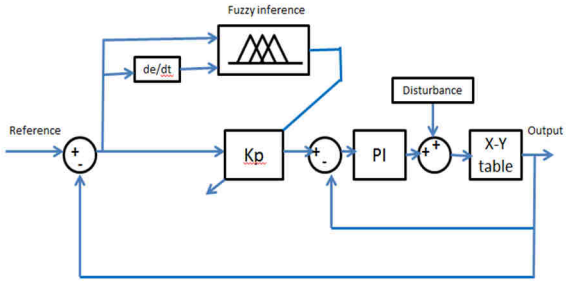

Figure 2 Structure of Cascade Fuzzy P+PI controller

The fuzzy control rules were designed based on the characteristics of the XY Table Ball Screw Driven System and properties of the Cascade P+PI controller. The rules of ΔKp were designed according to the 7x7 matrix. Suppose the variable range of the parameter Kp is $[Kp_{min}, Kp_{max}]$, the range of this parameter selected in this research is $Kp \in [281,283]$. This range can be calibrated over the interval [0, 1] as shown below:

$$Kp' = \frac{Kp - 281}{283 - 281} \quad (1)$$

Therefore, the value of proportional gain Kp can be obtained using the following equation (2):

$$Kp = 2Kp' + 281 \quad (2)$$

The system has been tested with sinusoidal input, where the frequency is set to three different values that are 0.3 Hz, 0.5 Hz, and 0.7 Hz. The amplitude for each set of

input signal is 10 mm and the system was run for 40 seconds. The measured cutting forces were inserted prior to the system as disturbance cutting forces. The tracking performance of the PI, Fuzzy PI, and Cascade Fuzzy P+PI controllers were analyzed and evaluated based on their performance against different cutting conditions.

3. RESULTS AND DISCUSSIONS

The results indicate that the improvement occurs when the value of *Kp* is tuned online using the fuzzy logic technique. It can be seen from the result that the improvement is about 33.7%. The improvement is more significant when the proposed Cascade Fuzzy P+PI is employed to the system, in which the improvement is about 70.9% and 56% with respect to the system with PI and Fuzzy PI, respectively. The performance of the system for each method is shown in Figure 3.

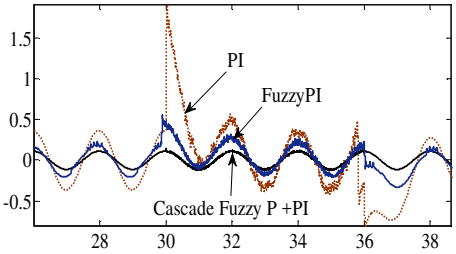

Figure 3 Comparison of the performance based on tracking error for the system with different controllers

As expected the system with the Cascade Fuzzy P+PI controller produced better performance compared to the other methods that are tested in this study. Table 1 shows the performance of the system with the proposed controller for difference speeds and frequencies.

Table 1 Cascade Fuzzy P+PI with disturbance

Spindle Speed	**Maximum Error [mm]**			**Tracking Percentage Error% =** $\frac{\text{Tracking Error}}{\text{Amplitud}} \times 100\%$		
Speed (rpm)/Freq (Hz)	**0.3**	**0.5**	**0.7**	**0.3**	**0.5**	**0.7**
0	0.066	0.111	0.156	0.66	1.11	1.56
1000	0.082	0.124	0.172	0.82	1.24	1.72
2000	0.085	0.127	0.173	0.85	1.27	1.73
3000	0.096	0.134	0.181	0.96	1.34	1.81

Figure 4 shows the variation of proportional gain *Kp* that is produced by fuzzy logic control. Figure 5 indicates the performance of the system with different controllers and spindle speeds that have been tested in this research. It is observed from this bar chart, the fuzzy logic control used to tune the proportional gain has reduced the tracking error substantially for all spindle speed cases.

4. CONCLUSIONS

Cascade Fuzzy P+PI controller was applied to the XY Table Ball Screw Driven System. This controller was used to improve the tracking performances of the system by minimising the tracking error, especially when the cutting force was applied at 1,000, 2,000, and 3,000 rpm spindle speed rotation. The sinusoidal input was applied as a reference and the frequency was set to three different values of 0.3 Hz, 0.5 Hz, and 0.7 Hz. The performance was then compared to other methods, namely PI and Fuzzy PI controllers. The research successfully demonstrated that the performance of the system with the Cascade Fuzzy P+PI controller is better than the other methods, where the improvement is about 70.9% with PI and Fuzzy PI, respectively.

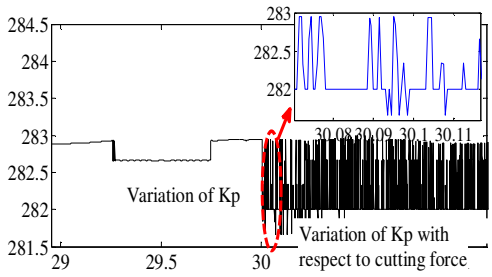

Figure 4 Variations of Kp based on Fuzzy tuning for the system with Cascade P+PI controller

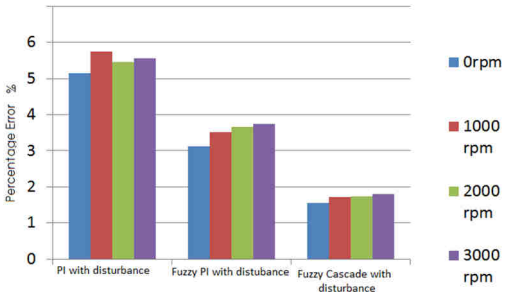

Figure 5 Performance of the system with different control techniques

REFERENCES

[1] F. Huo and A.N. Poo, "Precision contouring control of machine tools," *Int. J. Adv. Manuf. Technol.*, vol. 64, no. 1–4, pp. 319–333, 2013.

[2] K.K. Ahn and D.Q. Truong, "Online tuning fuzzy PID controller using robust extended Kalman filter," *J. Process Control*, vol. 19, no. 6, pp. 1011–1023, 2009.

[3] L.B. Zhang, Y.P. You and X.F. Yang, "A control strategy with motion smoothness and machining precision for multi-axis coordinated motion CNC machine tools," *Int. J. Adv. Manuf. Technol.*, vol. 64, no. 1–4, pp. 335–348, 2013.

[4] L. Abdullah, Z. Jamaludin, Q. Ahsan, J. Jamaludin, N. A. Rafan, C. T. Heng *et. al* "Evaluation on Tracking Performance of PID , Gain Scheduling and Classical Cascade P / PI Controller on XY Table Ballscrew Drive System Faculty of Manufacturing Engineering , Universiti Teknikal Malaysia Melaka (UteM)," *World Appl. Sci. J.*, vol. 21, pp. 1–10, 2013.

[5] P. Maji, S.K. Patra and K. Mahapatra, "Design and Implementation of Fuzzy Approximation PI Controller for Automatic Cruise Control System," *Adv. Artif. Intell.*, vol. Preprint, pp. 1–7, 2015.

Effects of citrate to nitrate ratio on superconducting properties of $YBa_2Cu_3O_{7-\delta}$ prepared via auto-combustion reaction

M.S. Mohd Suan[1]*, K.T. Lau[1], L.S. Chung[1], M.R. Johan[2]

[1)] Carbon Research Technology Research Group, Advanced Manufacturing Centre, Faculty of Manufacturing Engineering, Universiti Teknikal Malaysia Melaka, Hang Tuah Jaya, 76100 Durian Tunggal, Melaka, Malaysia
[2)] Nanomaterial Engineering Research Group, Advanced Materials Research Laboratory, Department of Mechanical Engineering, University of Malaya, 50603 Kuala Lumpur, Malaysia

*Corresponding e-mail: mohdshahadan@utem.edu.my

Keywords: $YBa_2Cu_3O_{7-\delta}$ superconductor; citrate-nitrate; auto-combustion

ABSTRACT – A series of $YBa_2Cu_3O_{7-\delta}$ was prepared via citrate-nitrate auto-combustion reaction. Metals nitrates were mixed with calculated amount of citric acid to obtain gels with citrate to nitrate ratio, c/n ranged from 0.3 to 0.9. The gel was transformed to fine ashes through auto-combustion reaction to yield $YBa_2Cu_3O_{7-\delta}$ during calcination. The XRD analysis revealed that each sample yielded orthorhombic polycrystalline of $YBa_2Cu_3O_{7-\delta}$ which was confirmed by EDX analysis. Each samples achieved zero resistivity in different manners. Samples with c/n = 0.3 and 0.5 behave more like normal metallic while samples with c/n = 0.6, 0.7 and 0.9 behaved like semiconductor.

1. INTRODUCTION

Yttrium barium copper oxide ($YBa_2Cu_3O_{7-\delta}$) is classified as high temperature superconducting material due to its ability to achieve zero electrical resistivity at temperatures above 77 K. Discovered in 1987, the critical temperature, T_C of $YBa_2Cu_3O_{7-\delta}$ synthesized using solid state reaction was found to be ~93 K [1]. This reaction however consumes a lot of time and energy since the precursor powders need to be ground repeatedly to achieve homogeneous mixture and requires higher calcination temperature to yield $YBa_2Cu_3O_{7-\delta}$ phase. Hence there have been many attempts to develop new synthesis method to obtain highly pure $YBa_2Cu_3O_{7-\delta}$ [2]. One interesting method that can be employed is citrate-nitrate auto-combustion reaction which is a powerful technique to obtain high purity samples since the reaction generates enough heat to volatize all low boiling point impurities [3]. The reaction is also having low processing costs, simple exothermic reaction, and can be used to yield new materials. The mechanism of the auto-combustion reaction is quite complex and highly influenced by citrate to nitrate ratio, c/n. Li et al. [4] in their study on synthesis of Al_2O_3 reported that excess or limited amount of citric acid results in different characteristics of combustion reaction which may produce impurities. Meanwhile Chandradass and Kim [5] had proposed that the optimum combustion reaction could occur when the oxidizer (metal nitrates) and fuel (citric acid) is stoichiometrically balanced. Thus, the effects of c/n towards the structural and superconducting properties of $YBa_2Cu_3O_{7-\delta}$ needed to be studied. In this work, the citrate-nitrate auto-combustion reaction was used to synthesize $YBa_2Cu_3O_{7-\delta}$ nanoparticles and the effects of c/n ratio were discussed.

2. METHODOLOGY

Analytical grade of $Y(NO_3)_3{\cdot}6H_2O$, $Ba(NO_3)_2$, and $Cu(NO_3)_2{\cdot}3H_2O$ reagent powders were dissolved in distilled water to prepare 0.5, 0.25 and 0.5 M of Y, Ba and Cu nitrate aqueous solutions respectively. These solutions then were mixed together by the mole ratio of Y:Ba:Cu = 1:2:3. An appropriate amount of citric acid was added into the mixture to alter the citrate-nitrate ratio, c/n value from 0.3 to 0.9 and its pH was adjusted to pH≈7 by adding liquor ammonia. Resultant solution then was dried at 250 °C on the hot plate with infrared lamp on top to provide uniform heating. After the auto-combustion reaction occurred, the as-prepared ashes powder was calcined at 900 °C under ambient atmosphere for 1 hour and let in the furnace cooling. The X-ray diffraction (XRD) for the calcined powder phase identification and crystallite size estimation was carried out using Ni-filtered Co Kα radiation by Bruker D8-advanced XRD machine. The peak position and intensities were obtained between 20° and 70° with a velocity of 0.02° s^{-1}. Energy dispersive X-ray (EDX) from Zeiss Ultra 40XB, was used to determine elemental distribution in the powder. The critical temperature, T_C, of the samples was measured using 4 point probe at liquid nitrogen temperature.

3. RESULTS AND DISCUSSIONS

Figure 1 shows the XRD patterns of $YBa_2Cu_3O_{7-\delta}$ samples with different c/n ratio. Vertical bars at bottom of the figure represent Bragg's diffraction angle of standard $YBa_2Cu_3O_{7-\delta}$ with lattice constants of a = 0.3877, b = 0.3827 and c = 11.6880 Å with Pmmm 47 symmetry. Each XRD pattern indicates the existence of polycrystalline $YBa_2Cu_3O_{7-\delta}$ phase. It can be observed that the XRD peaks for c/n = 0.6 and 0.7 samples occur at exact positions for standard $YBa_2Cu_3O_{7-\delta}$ phase prepared by Pathack et al. [1]. Few impurity peaks indicated by black dots in Figure 1 can be detected on XRD patterns of the samples with c/n = 0.3, 0.5 and 0.9 where these peaks can be assigned to YBaO and BaCuO phases. The atomic number of each element in each sample is listed in Table 1. From the atomic ratio of all samples, it was confirmed that samples with c/n = 0.6 and 0.7 had yielded pure $YBa_2Cu_3O_{7-\delta}$ compound. This is in good agreement with the XRD data. While the existence of excess Y, Ba and Cu in samples with c/n = 0.3 and 0.5 is the evidence of the presence of YBaO and BaCuO

impurities. The BaCuO impurity was also apparent in sample with c/n = 0.9 as the ratio of Ba exceeded the expected value.

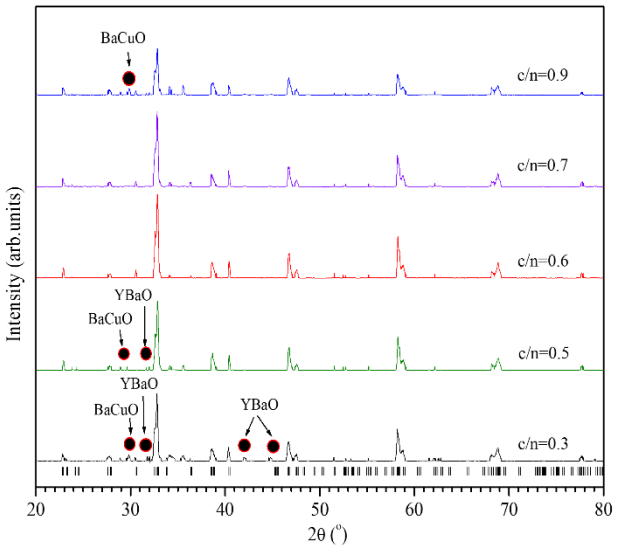

Figure 1 XRD patterns of $YBa_2Cu_3O_{7-\delta}$ samples after being calcination process

Table 1 EDX analysis of the $YBa_2Cu_3O_{7-\delta}$ samples

Sample (c/n)	Atomic (at. %)				Atomic Ratio
	Y	Ba	Cu	O	Y:Ba:Cu
0.3	11.27	14.13	17.66	56.93	1:1.25:1.57
0.5	11.75	13.51	18.07	58.67	1:1.15:1.54
0.6	8.37	16.83	24.38	51.02	1:2.01:2.91
0.7	8.20	16.45	24.67	50.67	1.0:2.0:3.0
0.9	6.89	16.95	19.12	57.04	1:2.46:2.78

Figure 2 shows the temperature dependence of electrical resistivity for $YBa_2Cu_3O_{7-\delta}$ samples with different c/n values. As can be seen from this figure, the resistivity of each sample was reduced to zero in different manners. The resistivity is decreased and stabilized before abruptly reduced to zero in c/n = 0.3 and 0.5 samples. At temperature above the T_C, the relation between resistivity and temperature of these samples is more likely normal metallic behavior. On the other hand, samples with c/n = 0.6, 0.7 and 0.9 were behaved like semiconductor as the resistivity is consistently decreased and then rapidly dropped to zero at the T_C. Inset in Figure 2 show the T_C onset and T_C zero values of the samples which are labelled by black and blue arrows respectively. The T_C onset is increased from 77.5 to 91.8 K as c/n is increased from 0.3 to 0.7. On the other hand, T_C onset decreased to 83.6 K in sample with c/n = 0.9. The T_C zero of the samples also vary by the same pattern. The transition widths are 2.5, 0.7, 1.0, 1.1 and 1.6 K for samples with c/n = 0.3, 0.5, 0.6, 0.7 and 0.9 respectively. The highest T_C zero is achieved in sample having c/n = 0.7 followed by the sample having c/n = 0.6. This is due to high purity of $YBa_2Cu_3O_{7-\delta}$ with oxygen deficiencies at around 0.2. Existence of non-superconducting YBaO and BaCuO impurities in samples having c/n = 0.3, 0.5 and 0.9 obstructed superconducting current to flow at T_C zero for typical $YBa_2Cu_3O_{7-\delta}$ superconductor.

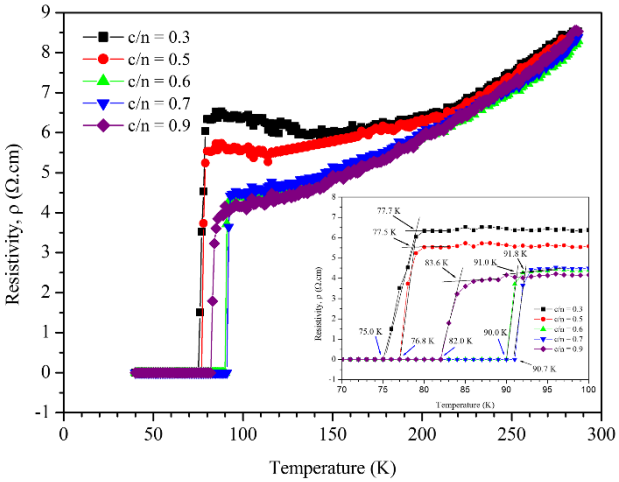

Figure 2 Temperature dependence resistivity of $YBa_2Cu_3O_{7-\delta}$ samples with different c/n. Inset shows T_C onset and T_C zero of the $YBa_2Cu_3O_{7-\delta}$ samples

4. CONCLUSIONS

The $YBa_2Cu_3O_{7-\delta}$ sample prepared using c/n = 0.7 was shown to have the highest purity compare to other samples. The sample exhibited T_C zero of 91.8 K with sharp transition width.

ACKNOWLEDGEMENT

Authors are grateful to Universiti Teknikal Malaysia Melaka for the financial support through PJP Research Grant numbered PJP/2016/FKP-AMC/S01499.

REFERENCES

[1] L.C. Pathak, S.K. Mishra, D. Bhattacharya and K.L. Chopra, "Synthesis and sintering characteristics of YBa–Cu-oxide superconductors", *Mater. Sci. Eng. B*, vol. 110, pp. 119–131, 2004.

[2] X. Wei, R.S. Nagarajan, E. Peng, J. Xue, J. Wang, J. Ding, "Fabrication of $YBa_2Cu_3O_{7-x}$ (YBCO) superconductor bulk structures by extrusion free forming", *Ceram. Int.,* vol. 42, no. 14, pp. 15836-15842, 2016.

[3] M.S. Mohd Suan and M. R. Johan, "Microhardness of Al_2O_3 nanoparticles added $YBa_2Cu_3O_{7-\delta}$ superconductor prepared using auto-combustion reaction", *Mater. Res. Inno.,* vol. 18, pp. 73-77, 2014.

[4] J. Li, Y. Wu, Y. Pan, and Ji. Guo, "Influence of citrate-to-nitrate ratio on the thermal behavior and chemical environment of alumina gel," *Ceram. Int.* vol. 33, pp. 735–738, 2007.

[5] J. Chandradass and K.H. Kim, "Effect of acidity on the citrate-nitrate combustion synthesis of alumina-zirconia composite powder", *Met. Mater. Int.* vol. 15, pp. 1039-1043, 2004.

A conceptual design of an interpreter for an open architecture control system

N.M. Seman, Z. Jamaludin*, M. Minhat, M.A. Othman

Faculty of Manufacturing Engineering, Universiti Teknikal Malaysia Melaka, Hang Tuah Jaya, 76100 Durian Tunggal, Melaka, Malaysia

*Corresponding e-mail: zamberi@utem.edu.my

Keywords: Interpreter; Control System; Simulink

ABSTRACT – In this paper, an interpreter for an open architecture control system is conceptually designed and proposed. The proposed method for the interpreter will allow the current control system to read input data file in the form of geometrical drawing, instead of some limited input source read in MATLAB / Simulink platform. The main aim of this paper is to propose a conceptual framework architecture design for an interpreter. The implementation of this interpreter will enable some functions (most of the functions are automatically generated from the software) that would link and interface geometrical data file in CATIA form and enable the converted position data to be read in Simulink environment. In future, the new interpreter will be applied with existing control system in Simulink domain.

1. INTRODUCTION

This article focuses to propose a conceptual framework architecture design for an interpreter. The existing system setup consists of a milling machine XY positioning table (utilizes a PC-based control to generate all controller signals) produced by Googol Tech [1]. Currently, the XY positioning table is controlled using in-house built controller designed and implemented in MATLAB/Simulink workspace. The existing controller uses its desired input to move its positioning table. According to Abdullah et. al. [2], and Jamaludin et al. [3], the control system applications are limited to simple forms of input signals by the Simulink input source blocks; such as sine, step, ramp and others as shown in Figure 1.

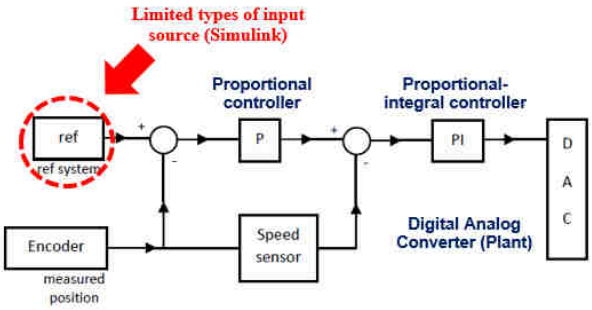

Figure 1 Block diagram for current control system's limitation

In order to further improve the existing control system in term of input form variations, a method is proposed that would enable reading of other types of input form based on given geometrical drawing using Computer Aided Design (CAD). Currently, there exist limited knowledge and know-how on product data exchange between CATIA and Simulink data. Thus, an interpreter is desired.

An interpreter is a program which can read input from any source code and is able to translate the codes to instructions. From the past ten years, several researches have been performed with regards to the development of platforms for interpreters. Liu et al. [4] used Java and Java 3D, Abdul-rani et al. [5] used Visual Basic dot NET, Ridwan et al. [6] used ST-Developer and VC++ and Mohamed et al. [7] used the integration of ST-Developer, NetBeans IDE, and IEC 61499 Function Blocks Editor. Even though researchers need to plug-in several software, yet it is more adaptable since the software has illustrated features. Thus, it is friendly-user rather than using the programmable-based software.

Therefore, in this paper, the interpreter can be understood as a translator between CATIA and MATLAB/Simulink. It reads neutral file from CATIA, interprets the data and then transfers it to MATLAB/Simulink. The methodology and expected result of this research are explained and discussed in Section 2 and 3 of this paper.

2. METHODOLOGY

This research is started with preliminary studies. The research problem is discovered and then literature reviews are conducted to obtain the research gap regarding developing platform trends. The gap then becomes the benchmark in solving the research problem which is how to translate from CATIA data to Simulink data.

The process flow for architecture framework design is illustrated in Figure 2. There are four phase involved to design the interpreter: (i) geometrical design and generation of STEP data, (ii) programming language conversion, (iii) machining setup graphical user interface (GUI), and (iv) integration of interpreter with current control system.

The geometrical drawing designed in CATIA automatically generated the STEP data with *.stp format. The *.stp data is in EXPRESS programming language. It is converted to Java language by using ST-Developer software. A machining setup GUI designed in NetBeans IDE will load the Java file and create output in form of Java Archieve (JAR) file. The JAR file was

programmed within MATLAB programming before it was defined in Simulink workspace. This system would then be interfaced with ControlDesk software.

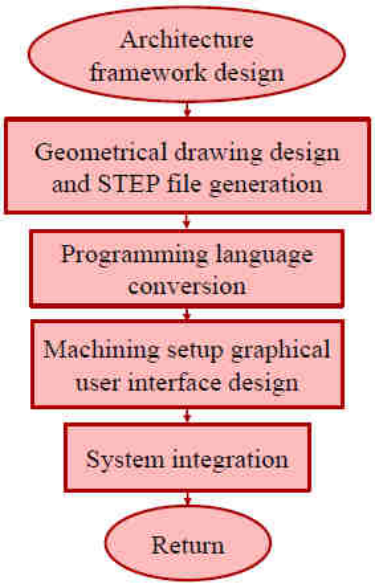

Figure 2 Architecture framework design process flow

3. EXPECTED RESULTS AND DISCUSSIONS

Figure 3 depicts the architecture framework design of the interpreter. CAD model designed in CATIA will be automatically generated as *.stp data. This file will be converted to Java by using ST-Developer software. This software has its own library which able to do the conversion. As to complete the interpreter, an interface is needed (designed in NetBeans IDE). The interpreter is integrated with current control system. This framework is one alternative to exchange product data between CATIA and MATLAB/ Simulink data.

The new control system is expected to have input in forms of CAD model. The new proposed input will be applied with basic controller design such as cascade P-PI and proportional-integral derivative (PID).

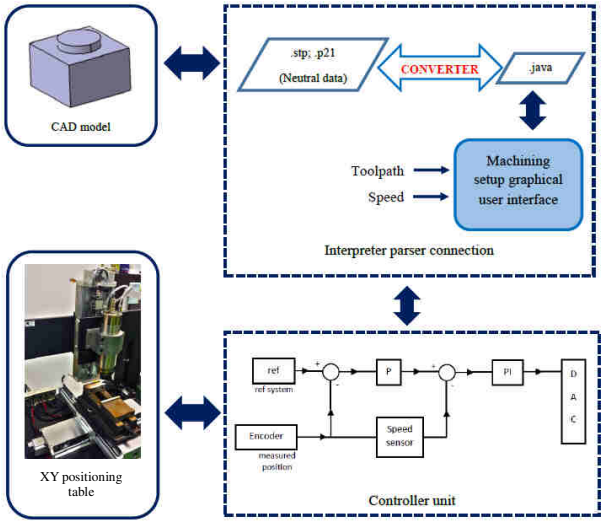

Figure 3 Architecture framework design for interpreter

4. CONCLUSIONS

As a conclusion, this paper proposed an alternative framework that links and interprets CAD drawings with position controllers previously designed in MATLAB/Simulink environment. This framework is theoretically analyzed by referring the scholars. In future, the proposed control architecture utilizing the designed interpreter is to be practically implemented and validated using the actual system. The implementation of this technology would enhance the capability of the existing control system contributing a step closer to the development of an in-house built CNC machine.

ACKNOWLEDGEMENT

The authors would like to thank the Ministry of Higher Education for the funding of this research with the references number FRGS/1/2015/TK03/FKP/02/F00281. The authors would like to thank the Faculty of Manufacturing Engineering and Universiti Teknikal Malaysia Melaka for the facilities provided.

REFERENCES

[1] "XYZ Stage," 2007. [Online]. Available: http://www.googoltech.com/web/eng/product_details_frame.jsp?gid=1327&module=Educational Products. [Accessed: 13-Jan-2016].

[2] L. Abdullah, Z. Jamaludin, M.N. Maslan, J. Jamaludin, N.A. Rafan and T.H. Chiew, "Assessment on Tracking Performance of Cascade P / PI , NPID and NCasFF Controller for Precise Positioning of XY Table Ballscrew Drive System," *Procedia CIRP*, vol. 26, pp. 212–216, 2015.

[3] Z. Jamaludin, H. Van Brussel, and J. Swevers, "Design of a Disturbance Observer and Model-based Friction Feedforward to Compensate Quadrant Glitches," *Motion and Vibration Control*, pp. 143–154, 2009.

[4] R.L. Liu, X.Z. Zhang and C.R. Zhang, "Design and Implementation of a Data Processing and Visualization System for STEP-NC Programs," *Appl. Mech. Mater.*, vol. 16–19, pp. 1015–1019, 2009.

[5] A.M. Abdul-rani, M. Gizaw, and Y. Yusof, "STEP Implementation on Turn-mill Manufacturing Environment," *Int. J. Mech. Aerospace, Ind. Mechatron. Manuf. Eng.*, vol. 5, no. 12, pp. 47–52, 2011.

[6] F. Ridwan, X. Xu and G. Liu, "A framework for machining optimisation based on STEP-NC," *J. Intell. Manuf.*, vol. 23, no. 3, pp. 423–441, 2012.

[7] S.B. Mohamed, A. Jameel and M. Minhat, "A Review on Intelligence STEP-NC Data Model and Function Blocks CNC Machining Protocol," *Adv. Mater. Res.*, vol. 845, pp. 779–785, 2014.

Photocatalytic activity of titania modified kenaf fiber as methylene blue purification process

O. Edynoor [1,2,3], T. Moriga [1,2*], K. Murai [1], A.R.M. Warikh [2,3]

[1)]Department of Chemical Science and Technology, Graduate School of Advanced Technology and Science, Tokushima University, 2-1 Minami-Josanjima, 770-8506 Tokushima, Japan
[2)]Tokushima-UTeM Academic Center, Tokushima University, 2-1 Minami-Josanjima, 770-8506 Tokushima, Japan
[3)]Department of Materials Engineering, Faculty of Manufacturing Engineering, Universiti Teknikal Malaysia Melaka (UTeM), Hang Tuah Jaya, 76100 Durian Tunggal, Melaka, Malaysia

*Corresponding e-mail: moriga@tokushima-u.ac.jp

Keywords: Photocatalytic; titania; kenaf

ABSTRACT – In this study, the effect of calcination temperature of titania (TiO_2) modified kenaf fiber (KF) is further explained. Immersion and sonication method have been applied to attach TiO_2 on KF surfaces. It is followed by drying at 90 – 100 °C for 3 h, and then calcination process is conducted for the conversion of $Ti_4^+ \rightarrow TiO_2$. The calcination temperatures are 100 °C, 125 °C and 150 °C. Photocatalytic activity is measured by Methylene Blue (MB) removal under UV irradiated time for 19 h. As a result, it shows that KF-TiO_2 with 100 °C calcined temperature is optimum with 90 % of MB removal, where constant MB removal rate is 0.5 % per irradiated hour. Finally, SEM-EDX images clearly show that TiO_2 exists on the KF surface.

1. INTRODUCTION

The commercial use of TiO_2 as photocatalyst is becoming widespread in the areas of water purification air purification, sterilization/disinfection and systems involving applications of the recently reported superhydrophilic effect [1]. In general, photocatalytic activity by TiO_2 (anatase and rutile phase) will be activated with the visible of UV light. However, for pure phases it is generally accepted that anatase exhibits a higher photocatalytic activity compared to rutile TiO_2 because of band gap differences [2].

The aims of study are to attach TiO_2 on KF at different calcination temperature and its photocatalytic application. In addition, hydrophilic nature of KF is playing important role for desorption and absorption mechanism for water purification. This situation could be enhanced KF-TiO_2 performance during purification process.

2. METHODOLOGY

In this work, the precursor solution was a mixture of 5ml titanium isopropoxide, TTIP (97 %, supplied by Aldrich Chemical) and 15 ml isopropanol (99 %, supplied by Merck). A 250 ml solution of de-ionized (D.I) water was used as the hydrolysis catalyst. The desired pH value of the solution was adjusted by adding HNO_3 for acidic solution. Then, the mixture underwent vigorous magnetic stirring for 24 h with 700 rpm at 70 °C. As a result, suspension white blue and high viscosity colloidal was obtained. Kenaf bast fibers used in this study were supplied by Innovative Pultrusion Sdn. Bhd. and were received in a form of randomly oriented mats with a surface density of 800 g/m^2. KF was alkaline treated by 5 % concentration of sodium hydroxide and dried at 80 °C for 3 h. Then, treated KF was immersed in TiO_2 solution for 30 minutes with sonication. After being immersed, it was then dried at 90 - 100°C in a vacuum oven for 3h. The samples were being washed by D.I water under sonication for 15 - 30 minutes to remove TiO_2 particles from KF. Finally, the sample was calcined at 100 °C, 125 °C and 150°C for 2 h. For photocatalytic activity test, mixture of KF-TiO_2 and MB solution with ratio 1g : 300 ml were stirred for 1h under dark condition for adsorption–desorption equilibrium. After that, it was exposed to UV irradiation light [3]. Then, the samples were characterized by XRD (2θ, 20 - 80 °) and UV spectrophotometer (500 – 700 nm wavelength) for TiO_2 phase detection and mechanism of MB removal respectively. SEM-EDX with x1000 magnification was carried out to discover TiO_2 on kenaf fibre (KF) surfaces.

3. RESULTS AND DISCUSSION

3.1 XRD spectroscopy result

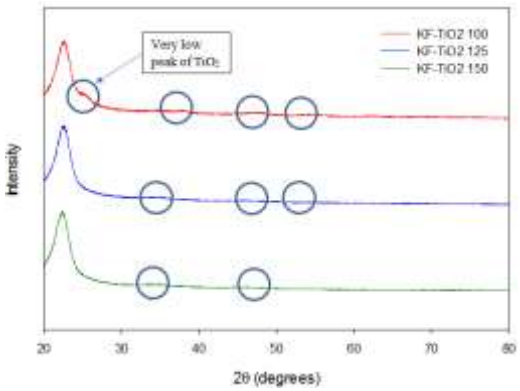

Figure 1 XRD results for 3 different calcined temperatures (100 °C, 125 °C and 150 °C)

As shown in Figure 1, KF-TiO_2 calcined at 100 °C was predominantly amorphous with a very small content of anatase crystallites of small crystalline size as broad, weak anatase-associated peaks were observed. However, coatings on KF did not show a crystalline phase. It might be due to the small content of anatase crystallites of small crystalline size. So, the peak was very broad, hence the intensity is small [4]. The overall percentage of TiO_2 occurred is about 6-8 %.

Consequently, it would affect the photocatalytic activity of KF-TiO_2 in MB purification process.

3.2 UV Spectrophotometer

Figure 2 shows the MB removal through absorption and desorption equilibrium and photocatalytic activity. It can be seen that calcined temperature had affected the degradation of MB. The % transmission of MB was at wavelength of 500 - 700 nm with interval time was increased when the TiO_2 and UV radiation present together. The highest transmission of MB degraded during photocatalytic activity was shown by the sample of KF-TiO_2 annealed at 100ºC with optimum rate was 0.5 % per irradiated hour, which was in line with the XRD result. During absorption and desorption equilibrium, KF-TiO_2 showed tremendous superhydrophilicity that absorbed about 70 % of MB while another 30 % remaining MB was removed during the photocatalytic activity. Thus, it can be said that hydrophilicity of KF and photocatalytic activity by TiO_2 were two main factors that involved during MB purification process.

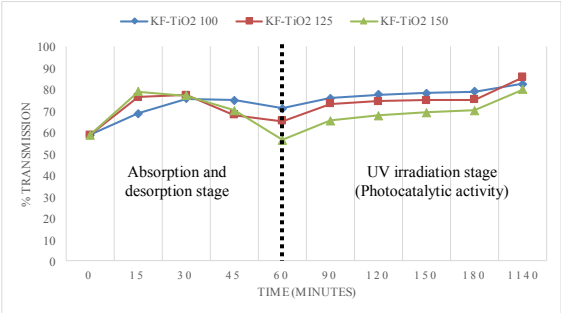

Figure 2 UV spectrophotometer results for 3 different calcined temperatures

Figure 3 MB solution color changes by presence of KF-TiO_2 (0,15,30,45,60,90,120,150,180 and 1140 minutes)

Figure 3 shows the MB solution color was changed during purification process. It indicated the involvement of KF-TiO_2 in MB purification process.

3.3 SEM-EDX images analysis

As illustrated in Figure 4, Ti^{2+} existed and coated around KF. The SEM-EDX analysis of KF-TiO_2 revealed the presence of C (red), O (green), and Ti (blue). C was modified by KF, O was modified by surrounding environment and considered as impurities while Ti^{2+} was modified by TiO_2. It was clearly seen that Ti^{2+} only existed on the KF surfaces instead of KF core. This situation confirmed that Ti^{2+} had been directly involved in photodegrading of MB.

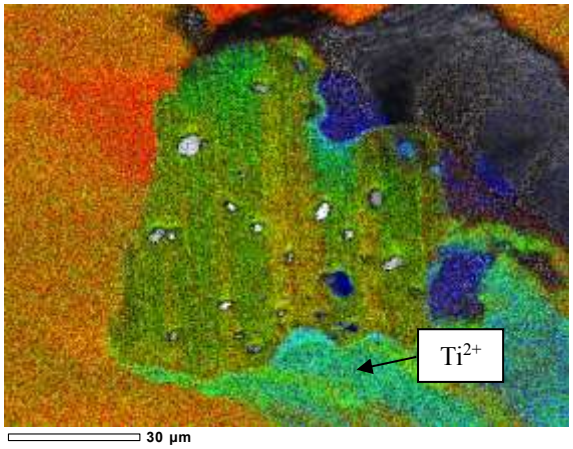

Figure 4 SEM-EDX cross sectional images for KF-TiO_2 : Ti^{2+} detection

4. CONCLUSIONS

TiO_2 was successfully coated kenaf fiber and could be functioned as photocatalyst reaction material. Hydrophilic properties of KF showed the ability of desorption and absorption mechanism of MB solution. The effect of calcination temperature of KF-TiO_2 was significantly reflecting the photocatalytic activity. The result showed that KF-TiO_2 with 100 ºC calcined temperature was the optimum rate of MB removal, with 0.5 % per irradiated hour. Finally, KF-TiO_2 revealed that it involved in MB purification process by photocatalytic activity.

ACKNOWLEDGEMENT

This work was partly supported by a fund for the research unit invitation from UTeM to Tokushima-UTeM Academic Center, Tokushima University for the year 2015-2016.

REFERENCES

[1] A. Bozzi, T. Yuranova , I. Guasaquillo , D. Laub, and J. Kiwi, "Self-cleaning of modified cotton textiles by TiO_2 at low temperatures under daylight irradiation," *Chemistry*, vol. 174, pp. 156–164, 2005.

[2] L. Tim, H. Sandamali, T. Junguang, K. Alan, S. Eli Sutter and B. Matthias, "Why is anatase a better photocatalyst than rutile? - Model studies on epitaxial TiO_2 films," *Photocatalysis pollution remediation*, vol. 4, pp. 4043, 2014.

[3] S. Salmin and Al-Shamali, "Photocatalytic Degradation of Methylene Blue in the Presence of TiO2 Catalyst Assisted Solar Radiation," *Basic And Applied Sciences,* vol.7, no. 4, pp. 172-176, 2013.

[4] Q. Kaihong, A.Daoud Walid, H. Xin John, C. L. Mak, T. Waisze, and W. P. Cheunga, "Self-cleaning cotton," *Material Chemistry*, pp. 4567–4574, 2006.

Synthesis of graphene powders from hydrothermally produced nickel catalyst by using alcohol catalytic chemical vapor deposition

R.N.A.R. Seman[1*], M.A. Azam[1], R. Izamshah[1], G. Omar[2], S. Ismail[1], Z. Muslim[3], N. Mohamad[1], M.S. Kasim[1]

[1)] Carbon Research Technology Research Group, Advanced Manufacturing Centre, Faculty of Manufacturing Engineering, Universiti Teknikal Malaysia Melaka, Hang Tuah Jaya, 76100 Durian Tunggal, Melaka, Malaysia
[2)] GTriboE, CARe, Faculty of Mechanical Engineering, Universiti Teknikal Malaysia Melaka, Hang Tuah Jaya, 76100 Durian Tunggal, Melaka, Malaysia
[3)] Faculty of Information and Communication Technology, Universiti Teknikal Malaysia Melaka, Hang Tuah Jaya, 76100 Durian Tunggal, Melaka, Malaysia

[*]Corresponding e-mail: P051520003@student.utem.edu.my

Keywords: Nickel catalyst; graphene; alcohol catalytic chemical vapor deposition

ABSTRACT–Mass production of high-quality graphene powder is important for various applications. In general, graphene powders were produced on large industrial scale by chemical processes and liquid-phase exfoliation of graphite. However, strong-interaction-induced interlayer aggregation usually leads to the degradation of their intrinsic properties. Moreover, the crystallinity or layer-thickness controllability is not so perfect for advanced technologies. Here, we report a facile hydrothermal method to produce nickel (Ni) as catalyst to grow graphene by alcohol catalytic chemical vapor deposition (CVD). Different CVD processing times have been investigated in order to obtain the optimized condition for graphene synthesis. The as-prepared Ni was confirmed by X-ray diffraction (XRD). Meanwhile, the Raman spectrum shows that the optimized time for effective graphene synthesis is 5 min. This CVD system and the Ni catalyst are scalable and low cost, thus suitable for high quality graphene synthesis.

1. INTRODUCTION

Graphene, a two-dimensional planar single sheet of sp^2 hybridized carbon atoms arranged in a honeycomb lattice was first discovered by Novoselov and colleagues in 2004. Graphene has been widely used as electrode material due to its remarkable characteristic such as excellent electrical conductivity, good thermal and electrochemical properties [1,2]. Currently, many efforts have been made to prepare large quantity graphene sheets and their derived materials by chemical and liquid-phase exfoliation of graphite [3-5].

Alternatively, the graphene structures have been explored by CVD in which the crystallinity and thickness controllability of graphene layers can be greatly improved in this way [6,7]. While Ni as catalyst for graphene synthesis can be obtained by different ways [8], we have attempted to synthesis the Ni by a hydrothermal method using nickel nitrate as precursors. This method is suitable for the growth of good quality crystals while maintaining their composition. Also, it is simple to implement and scale up as well as allows controlling the particles size and properties [9].

Here we report a facile synthesis to grow multi-layer graphene powder by using alcohol catalytic CVD technique. The advantage of the CVD process is relatively low cost and the yield of graphene compared to that of reduced graphene oxide and liquid-phase exfoliated graphene sheets [10,11]. Different CVD processing time has been investigated in order to evaluate the optimum CVD processing parameter for the graphene synthesis.

2. METHODOLOGY

Ni powder was prepared using a hydrothermal method. 0.36 g of metal precursor nickel (II) nitrate hexahydrate (Sigma Aldrich, 99.999%) was dissolved into 100 ml of ethanol. The mixture was stirred for 10 minutes and then it was dried at 150 ºC for 12 hours. After cooling down, it was grinded to get a fine powder. The resulting Ni-O powder was further heated at 300 ºC for 2 hours. The graphene synthesis process was performed by using CVD system (MILA 3000). 200 mg of the Ni powder was dispersed on crucible alumina which was placed in the middle of the ceramic tube. The reactor was purged with Ar until the reactor reached 900°C and 2.25 Torr of CVD furnace. The use of ethanol as the carbon source in CVD method was to exhibit low reaction temperature and high purity level of the carbon products [12]. In order to get high yield graphene powder, CVD processing time was varied to 30s, 2 min, and 5 min. X-ray diffraction (XRD) equipped with Cu Kα radiation (λ = 0.15406 nm) was used to characterize the crystallographic structures of the Ni-O powder. The quality of obtained graphene was performed by Raman spectrum (Renishaw, λ= 532 nm).

3. RESULTS AND DISCUSSIONS

In order to confirm the phase formation and purity of the hydrothermal product, we have done powder XRD measurements. Figure 1 illustrates the XRD patterns of as-prepared hydrothermal product. XRD pattern reveals the cubic Ni-O (JCPDS: 47-1049) [13] with the observed peaks; (111), (002), (202), (113), and (222).

Figure 2 represents a typical Raman spectrum of the sample. For 5 min growth time, G-peaks and 2D-peaks are clearly visible at 1587 cm^{-1} and 2697 cm^{-1}, respectively. Meanwhile, there is no peaks were observed on the 30s and 2 min graphene synthesis time. This is relatively due to shorter CVD processing time for Ni to act as catalyst for the formation of graphene.

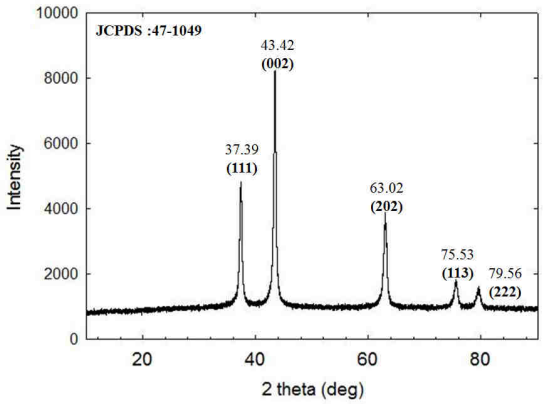

Figure 1 XRD pattern of the a as-prepared Ni-O powder

The relative intensity ratio of I_{2D}/I_G can be used to distinguish the number of layers of graphene sheets. The intensity ratio I_{2D}/I_G of 2, 1–2, and 1 correspond to single-layered, double-layered and multi-layered graphene, respectively [14]. No single-layered graphene sheet was identified by the Raman test. It can be concluded that this graphene was multi-layer graphene.

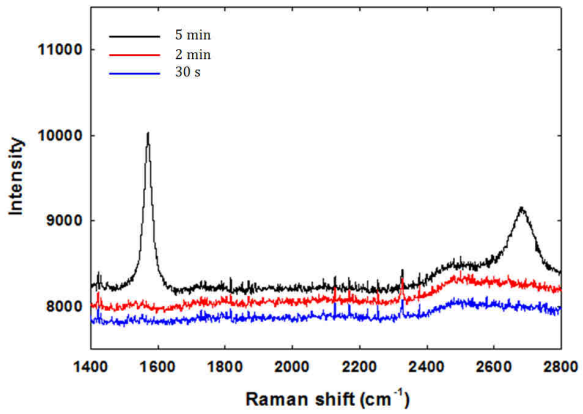

Figure 2 Raman spectrum of graphene

4. CONCLUSIONS

In conclusion, the graphene powder was successfully synthesized by using Ni as catalyst. In the synthesis of graphene powder by ACCVD method, the growth time plays a key role. The results showed that the formation of graphene growth was low at lower growth time and as the growth time increases, the graphene yield increases correspondingly. It can be concluded that, in this work, the optimum CVD processing time for the high yield graphene synthesis was 5 minutes. The longer graphene synthesis time eg: 10, 20, and 30 min might give a different result in graphene formation. Thus, it is critical for further investigation of the graphene synthesis with reflection to the desired amount of graphene powders yield and with the ability of CVD system. This CVD method has typically better electrical, produce high quality, high-performance, and other properties than chemically prepared graphene. Therefore, there is a need to develop a cost-effective scale-up manufacturing processes for high yield graphene using CVD method. The main contribution of this finding was CVD processing time, carbon as feedstock, CVD pressure, as well as catalyst.

ACKNOWLEDGEMENT

Authors are grateful to Universiti Teknikal Malaysia Melaka for the financial support through PJP High Impact Research PJP/2016/FKP/HI6/S10483. Also, R.N.A.R. Seman thanks to UTeM Zamalah Scheme for PhD financial support.

REFERENCES

[1] K.S. Novoselov, A.K. Geim, S.V. Morozov, D. Jiang, Y. Zhang, S.V. Dubonos *et. al*, "Electric field effect in atomically thin carbon films," *Science,* vol. 306, pp. 666-669, 2014.

[2] M.A. Azam, N. Dorah, R.N.A.R. Seman, N.S.A. Manaf, and T.I.T. Kudin, "Electrochemical performance of AC and graphene based supercapacitor," *Mater. Technol.* vol. 30, pp. A1-A4, 2015.

[3] T. Wu, X. Zhang, Q. Yuan, J. Xue, G. Lu, Z. Liu *et al.*, "Fast growth of inch-sized single-crystalline graphene from a controlled single nucleus on Cu–Ni alloys," *Nat. Mater.* pp. 1-6, 2015.

[4] L. Dai, "Functionalization of Graphene for Efficient Energy Conversion and Storage," *Acc. Chem. Res.* vol. 46, pp. 31−42, 2013.

[5] M.A. Azam, N.H. Jantan, N. Dorah, R.N.A.R. Seman, N.S.A. Manaf, T.I.T. Kudin *et al.*, *Mater. Res. Bull.* vol. 69, pp. 20-23, 2015.

[6] Z. Chen, W. Ren, L. Gao, B. Liu, S. Pei, and H.M. Cheng, *Nat. Mater.,* vol. 10, pp. 424−428, 2011.

[7] K. Yan, L. Fu, H.L. Peng, and Z.F. Liu, *Acc. Chem. Res.,* Vol. 46, pp. 2263-2274, 2013.

[8] S. Balamurugan, A.J.L. Philip, and R.S. Vidya, *J Supercond Nov Magn*, pp. 1-6, 2016.

[9] H. Hayashi and Y. Hakuta, *Materials*, vol. 3, pp. 3794-3817, 2010.

[10] K. Chen, Z. Chai, C. Li, L. Shi, M. Liu, Q. Xie, Y. Zhang, D. Xu, A. Manivannan, and Z. Liu, *ACS Nano*, vol. 10, pp. 3665−3673, 2016.

[11] M.A. Azam, A. Fujiwara, and T. Shimoda, *Int. J. Electrochem. Sci.*, vol. 8, pp. 3902-3911, 2013.

[12] S.M. Toussi, A. Fakhru'l-Razi, A.L. Chuah and A.R. Suraya, *Sains Malaysiana*, vol. 40, no. 3, pp. 197-201, 2011.

[13] L. Kang, J. Deng, T. Liu, M. Cui, X. Zhang, P. Li, Y. Li, X. Liu, W. Liang, *J. Power Sources*, vol. 275, pp.126-135, 2015.

[14] Y. Shen, and A.C. Lua, *Sci. Rep.,* vol. 3, pp. 3037 (1-6), 2013.

A concept of reconfigurable conveyor system in manufacturing system: logical reconfiguration

N.R. Mohamad, A.A.A. Rahman*, M.A.A. Rahman

Integrated Manufacturing System (I'MS) Research Group, Advanced Manufacturing Centre, Faculty of Manufacturing Engineering, Universiti Teknikal Malaysia Melaka, Hang Tuah Jaya, 76100 Durian Tunggal, Melaka, Malaysia

*Corresponding e-mail: azrulazwan@utem.edu.my

Keywords: Reconfigurable Conveyor System; Logical Reconfiguration; Programmable Logic Controller

ABSTRACT – Conveyor system is one of automated material handling system that commonly used in manufacturing industry. Due to the problem such as dynamic nature, space available and risk operation, these conveyor systems are unable to suit the current market requirement. Therefore, this paper aimed to propose a logical reconfiguration of Reconfigurable Conveyor System. The Programmable Logic Controller (PLC) is used as programming tool to develop the control strategies of Reconfigurable Conveyor System. The program is designed by using IEC 61131 protocol. In conclusion, the proposed program will be validated by using the Reconfigurable Conveyor System prototype.

1. INTRODUCTION

Manufacturing industries are now moving towards to an advance technology. A new type of manufacturing system is required in order to make the competitive between companies mostly in manufacturing industries to make it responsive to the market changes due to the unpredictable global changes [1]. Therefore, a new concept of Reconfigurable Conveyor System is adapted to convert the new model of production with cost effective and short time that offers significant flexibility in both hardware and software in order to support the sudden change of the market requirements and the change of the engineering technology [2]. The concept offers two type reconfigurations which are physical reconfiguration and logical reconfiguration. This paper proposes a concept of logical reconfiguration in Reconfigurable Conveyor System.

2. METHODOLOGY

The concept of logical development is designed by using Programmable Logic Controller (PLC). This is because PLC is easy to monitor the simulation of the controller. In addition, PLC is used to ensure the smooth transition, stability and accuracy of a manufacturing process [3, 4]. In this research, PLC is the main controller that is used to give instruction to all the equipment around the system. Figure 1 shows the overall flowchart of process flow in logical reconfiguration that is used in this research. The process is start by determining the sequence of operation of the reconfigurable conveyor system. This is because the control strategies must be suitable with the physical reconfiguration. After that, the main program in main system controller is developed. Then, the module of sub-system controller is selected based on the requirement program. Local Area Connection (LAN) cable is connected to the desired controller. After that, the program is uploaded and lastly the conveyor will be started. This step will be repeated until the testing achieved the desired system. The control strategies will be monitored through a computer. If there are any errors during the process operation, the program will provide a feedback to the monitor so that the person in charge is alerted and will be able to solve the problem immediately. When the emergency stop button is pushed, all the system will be stopped automatically.

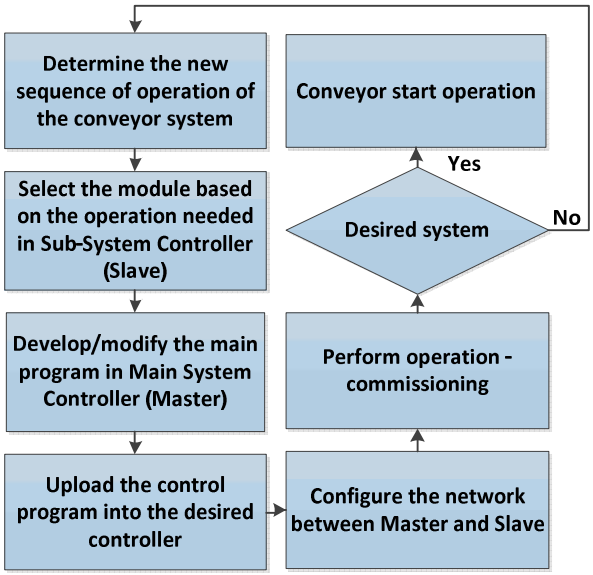

Figure 1 Overall Flowchart of process flow in Reconfigurable Conveyor System

3. RESULTS AND DISCUSSIONS

Reconfigurable Conveyor System consist six modules. Three modules are straight line belt conveyors and three modules are pneumatic conveyors. Each of modules has their own controller. For this research, there are two system controllers that are used. First is main system controller. It is used to control all the six modules of the Reconfigurable Conveyor System operation. Second is sub-system controller. It is used to control the operation that need to carry out in each module. Figure 2 shows the logical reconfiguration of Reconfigurable Conveyor System and some possible layout reconfiguration. There are three physical modules which are straight line conveyor (c1), pneumatic cylinder conveyor (c2) and combination between straight line conveyor and pneumatic cylinder conveyor (c3). The program of each module consists of different

numbers of sensor (SE), pusher (PU), pneumatic cylinder (CYL) and motor (M). Each program is designed by using IEC 61131 protocol. From the inputs and outputs in ladder diagram, it will be wired together with connection links to form a block. This process is also can be called as Function Block (FB). It is used as a graphical language to transfer data through block. One of the advantage of FB is it is easy to understand and being reusable software elements. The reusable FB is developed so that the user can easily put the value input and output based on the program requirement. In this research, FB is used to support the reconfiguration's concept to reduce time taken when layout of the conveyor system is changed. Each FB is designed with specific program to control the output of the Reconfigurable Conveyor System. For example, function of FB motor is to run the motor. FB1 is designed with three FB which are SE, PU and M for one module of conveyor system. From these FB, there are four possible layout reconfiguration that can be form which are single straight line, L-shaped, U-shaped and closed loop shaped. The concept is validated by using the Reconfigurable Conveyor System prototype.

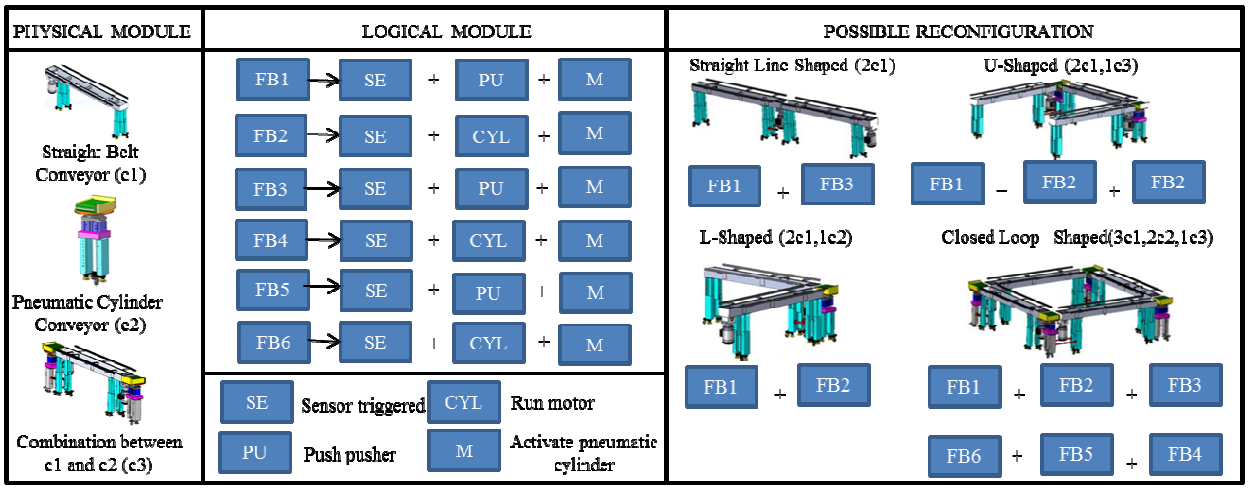

Figure 2 Logical Reconfiguration of Reconfigurable Conveyor System

From the experiment, the logical reconfiguration is validated by using Single Minutes Exchange Dies (SMED) analysis. SMED is one of lean production method to reduce the waste in operation. In this research, SMED is used to reduce time for one operation of Reconfigurable Conveyor System. Figure 3 shows some example of analysis that carried out by using logical reconfiguration of Reconfigurable Conveyor System. Based on the figure below, the total time taken of logical reconfiguration for one operation is 445.69 minutes.

	The Reconfigurable Conveyor System			
No.	Task/Operation	Time (min)		Frequency
		Internal	External	
1	Determine the sequence operation of the conveyor system	2.15		1
2	Switch on the power of the conveyor		37.02	6
3	Pull to open the pneumatic hose power		15.12	1
4	Pull to off the pneumatic hose power		15.12	1
5	Open CX-Programmer	8.05		1
6	Open new project - select new plc	102.22		1
7	Put LAN cable into Ethernet port in each PLC modules		72.9	6
8	Modify and added the desired Function Block (FB)	102.12		1
9	Load and transfer the program into the PLC module		15.69	1
10	Unload USB cable from the PLC		0	0
11	Push Start button to run the operation	75.3		6
	Time taken for one operation	289.84	155.85	25
	Total time: (Internal + External)	445.69		

Figure 3 Logical Reconfiguration Analysis

4. CONCLUSIONS

In conclusion, reconfiguration plays a critical role to support the new challenge in manufacturing industries. This logical reconfiguration is providing the reusable control strategies of the reconfigurable conveyor system. From the analysis, this concept shows that Reconfigurable Conveyor System can reduce time needed to program the controller when the layout needs to be change into the requirements.

REFERENCES

[1] Y. Koren and M. Shpitalni, "Design of reconfigurable manufacturing system," *Journal of Manufacturing System*, vol. 29, no. 4, pp.130–141, 2010.

[2] D. Nazzal and A. EL-Nashar, "Survey of research in modeling conveyor-based automated material handling systems in wafer fabs," *Proceedings of Winter Simulation Conference,* 2007, pp. 1781–1788.

[3] A.A.A. Rahman, *Approach for integration predictive-reactive job shop scheduling with PLC-controlled material flow*, Technischen Universitat Berlin, 2013.

[4] R. Lewis, *Modeling control system using IEC 61499*, The Institution of Engineering and Technology, London, United Kingdom, 2008.

Proceedings of Innovative Research and Industrial Dialogue'16, pp. 115-116 (May 2017)

Design and analysis of cascade P/PI controller for XY milling table ballscrew driven system

M. Maharof *, Z. Jamaludin, M. Minhat

Faculty of Manufacturing Engineering, Universiti Teknikal Malaysia Melaka, Hang Tuah Jaya, 76100 Durian Tunggal, Melaka, Malaysia

*Corresponding e-mail: madihah.maharof@yahoo.com.my

Keywords: Cascade P/PI Controller; Tracking Error; XY milling table

ABSTRACT – This paper focuses on design and analysis of a cascade P/PI controller for position control of an XY milling table ballscrew driven system. For design purposes, the measured, frequency response function (FRF) was used to represent the real system. Moreover, the parameters of the cascade P/PI controllers were chosen and tuned based on gain margin and phase margin considerations of the open loop transfer functions. First, the PI velocity loop controller parameters were designed and the loop characteristics analyzed. Second, the P position loop controller was designed and analyzed. Finally, the tracking performance of the cascade P/PI was analyzed with and without feedforward element for a sinusoidal reference input signal of amplitude 1mm and frequency 10Hz.

1. INTRODUCTION

Motion tracking controllers are designed with the objective of realising best possible tracking accuracy and precision in machining process [1, 2]. However, in most cases, the presence of disturbance forces led to inaccuracy and error amplification [3]. The amplitude of the tracking errors and the input signals are two important indicators to validate a good control system design.

This paper discusses design and performance analyses of classical cascade P/PI controller for position control of a ballscrew driven system. The tracking performance was analysed for control system with and without feedforward element.

2. METHODOLOGY

In this section, design of Cascade P/PI controller is carried out in a step-by-step procedure as shown in Figure 1. The system identification was performed based on measured FRF on the XY milling table. Figure 2 illustrates the schematic diagram of the experimental setup for system identification. The experimental setup for system identification consists of four main components, namely; a personal computer with MATLAB/Simulink and ControlDesk software, dSPACE DS 1104 Digital Signal Processing (DSP) board, an amplifier and a XY milling table ballscrew driven unit. A host computer fitted with ControlDesk software from dSPACE is integrated with the dSPACE DS 1104 digital signal processing (DSP) board. The DSP board is then linked to the servo amplifier of the plant (XY milling table). The host computer acts as a central control-processing unit providing necessary inputs to the plant and monitoring essentials feedbacks for effective control of the positioning table.

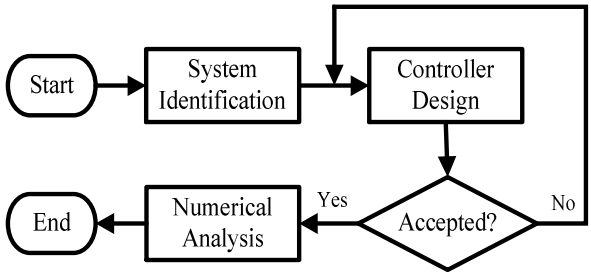

Figure 1 Flowchart of the controller design

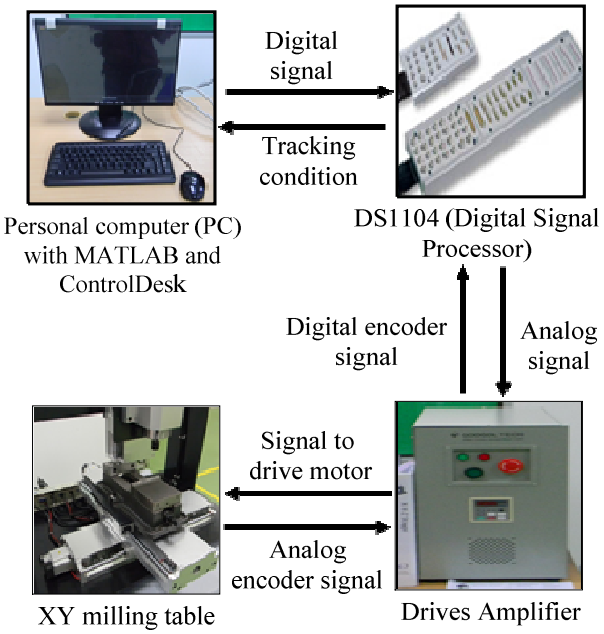

Figure 2 Schematic diagram of the experimental setup for system identification

3. RESULTS AND DISCUSSION

3.1 Design and Analysis of the Velocity Loop

The loops control parameters of the cascade P/PI controllers are designed and concluded based on gain margin and phase margin consideration of the respective open loop transfer functions. First, PI velocity loop controller parameters are designed and the loop shaping is determined based on control scheme shown in Figure 3.

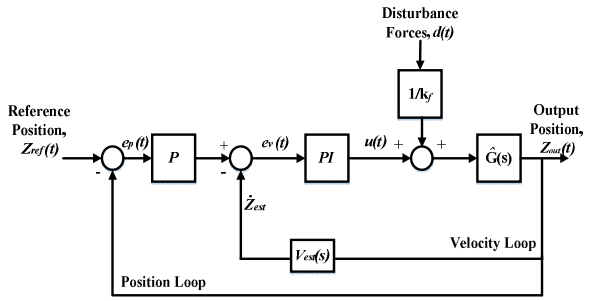

Figure 3 Frequency domain scheme of cascade P/PI controller

The velocity open loop and closed loop transfer functions are:

$$Vel_{ol} = \frac{\dot{Z}_{est}(s)}{E_v(s)} = PI.\hat{G}.V_{est} \quad (1)$$

$$Vel_{cl} = \frac{\dot{Z}_{est}(s)}{U_p(s)} = \frac{PI.\hat{G}.V_{est}}{1+PI.\hat{G}.V_{est}} \quad (2)$$

The velocity loop PI controller parameters, k_p and k_i are selected based on gain and phase margin consideration of the velocity open loop transfer function. A proper selection of the values for the gain margin and the phase margin is critical to guarantee stability and good transient response characteristics [4]. Table 1 lists the PI controller parameters.

Table 1 PI controller parameters

k_p [volt.s]	k_i [volt.s^2]
0.0005695	0.05306

3.2 Design and Analysis of the Position Loop

Second, the position open loop and closed loop characteristics are examined for a proportional gain controller k_v equals:

$$k_v = 540\text{s}^{-1} \quad (3)$$

Based on Figure 3, the position open loop and closed loop transfer functions are as follows:

$$Pos_{ol} = \frac{Z(s)}{E_p(s)} = \frac{P \cdot PI \cdot \hat{G}}{1+PI \cdot \hat{G} \cdot V_{est}} \quad (4)$$

$$Pos_{cl} = \frac{Z(s)}{Z_{ref}(s)} = \frac{P \cdot PI \cdot \hat{G}}{1+PI \cdot \hat{G} \cdot V_{est}+P \cdot PI \cdot \hat{G}} \quad (5)$$

Table 2 summarizes the gain margin and phase margin for the velocity open loop and position open loop transfer functions. These values ensure good transient response and stability.

Table 2 Gain margin and phase margin of velocity open loop and position open loop transfer function

Loops	Gain margin	Phase margin
Velocity	10.7 dB	82.2 deg
Position	4 dB	41.7 deg

3.3 Numerical Analysis of Tracking Performance

The tracking performance is evaluated based on position and tracking errors as shown in Figure 4. Table 4 lists the tracking error in terms of root mean square of error (RMSE). The performance was analyzed for a sinusoidal reference input signal of an amplitude 1mm and frequency of 10Hz.

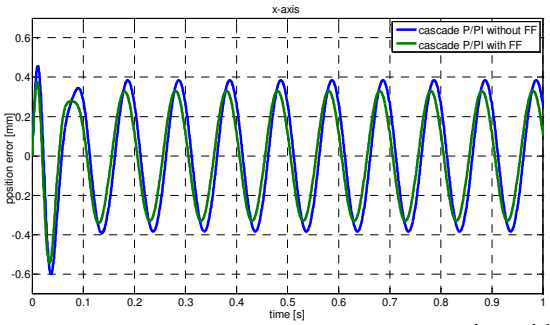

Figure 4 Numerical results of tracking error for sinusoidal reference signal of amplitude 1mm and frequency 10Hz

Table 4 RMSE tracking error of cascade P/PI and cascade P/PI with feedforward

Tracking error	Cascade P/PI [mm]	Cascade P/PI with feedforward [mm]
RMSE	0.2726	0.2343

4. CONCLUSIONS

As conclusion, this paper has shown that the cascade P/PI controller was successfully designed and applied, achieving the desired results. Velocity feedforward is applied at the velocity loop of the cascade P/PI controller resulting an improvement of tracking error in terms of root mean square of error (RMSE).

ACKNOWLEDGEMENT

The authors would like to thank the Ministry of Higher Education for the funding of this research with the reference number FRGS/1/2015/TK03/FKP/02/ F00281. The authors would also like to thank the Faculty of Manufacturing Engineering and Universiti Teknikal Malaysia Melaka for the facilities provided.

REFERENCES

[1] T. Moriwaki, "Multi-functional machine tool," *CIRP Annals-Manufacturing Technology,* pp. 736-749, 2008.

[2] S. Mekid and T. Ogedengbe, "A Review of Machine Tool Accuracy Enhancement Through Error Compensation in Serial and Parallel Kinematic Machines," *International Journal of Precision Technology*, vol. 1, no. 3, pp. 251-286, 2010.

[3] Z. Jamaludin, H.V. Brussel and J. Swevers, "Classical cascade and sliding mode control tracking performance for a XY table of a high-speed machine tool," *International Journal Of Precision Technology,* vol. 1, no. 1, pp. 65-74, 2007.

[4] P. Boucher, D. Dumur, K.F. Rahmani, " Generalized predictive cascade control (GPCC) for machine tool drives," *Annals of the CIRP*, vol. 39, no. 1, pp. 357-360, 1990.

Animal robot therapy for rehabilitation patients with major depressive disorder

W.Z. Zulkifli[1], S. Shamsuddin[1,*], T.H. Lim[2]

[1)] Faculty of Manufacturing Engineering, Universiti Teknikal Malaysia Melaka, Hang Tuah Jaya, 76100 Durian Tunggal, Melaka, Malaysia.

[2)] Psychosocial Department, SOCSO Rehabilitation Center, Bandar Hijau, Hang Tuah Jaya, Melaka, Malaysia

[*]Corresponding e-mail: syamimi@ieee.org

Keywords: human-robot interaction (HRI); robot therapy; Major Depressive Disorder (MDD)

ABSTRACT – Presently, the utilization of therapeutic animal robots has expanded. PARO is a robotic seal developed to give psychological effects on patients. One of PARO functions is to be used as an assistive device and possibly as an augmentation strategy with other Psychological interventions. Major Depressive Disorder (MDD) or simply known as Clinical Depression, is a common but severe mood disorder. This research work is focusing on the interaction protocol of therapeutic animal robot PARO with patients that fulfill either with provisional or full criteria of MDD. The outcome is to help patients by reducing their stress level through facilitated therapy session with a therapeutic animal robot.

1. INTRODUCTION

World Health Organization (WHO) has classified depression as a common illness worldwide, with an estimated 350 million people affected. In Malaysia, the prevalence is estimated between 8-10% of the population. Strong range of emotions on sadness and bereavement are often related to Clinical Depression or technically referred to as Major Depressive Disorder (MDD). MDD may disturb physiological functions due to the high level of stress and low mood. Potential consequences are increased blood pressure and changes in emotion [1]. Therefore, it is important to have interventions that can reduce stress and ruminative negative thinking. People who are exposed to medical-related fears settings is a vulnerable group of population that may experience a great level of stress [2]. Animal therapy is proven to have positive effects to relieve depression and anxiety. Currently, many studies have found benefit of companion animals to provide mental support.

Earlier studies showed that animals are capable of lowering stress, reducing heart and respiratory rate, and show positive changes in hormone level and as well mood elevation [3]. However, the use of animals has a number of drawbacks. In many therapy institutes, an animal is not readily available to the patients because it only takes place in a scheduled event. Animal therapy are also discouraged due to the fear of diseases, bites, or allergies. Robot therapy, specifically in mental health care through interactions with the robot has been studied by many researchers. Therapy through robot is expected to have physiological effects similar to animal therapy.

Figure 1 Therapeutic animal robot PARO

This research aims to use a therapeutic robot PARO (Figure 1) which focuses on human-robot interaction (HRI) method with PARO as a social companion.

2. METHODOLOGY

The experimental procedure serves as a platform to investigate changes in the stress level of patients with MDD before and after interacting with PARO robot.

2.1 Experiment Setup

Selection of patients depend on following criteria:

a. Age between 20-40 years old
b. Symptoms of Depression diagnosed/identified
c. Symptoms of Insomnia diagnosed/identified

The therapy session will be conducted at the SOCSO Rehabilitation Center located in Melaka. The therapy session will be conducted in a designated room where PARO robot will socialize with patients and assisted by a psychologist (Figure 2).

2.2 Experimental Procedure

The therapy procedure is divided into 2 sections:

a. Pre-experimental
b. Therapy session

2.2.1 Pre-experimental Procedure

The procedure starts with describing the session experimental procedure to patients along with the documents. The patients who agree to participate will need to sign a consent form, indicating their willingness

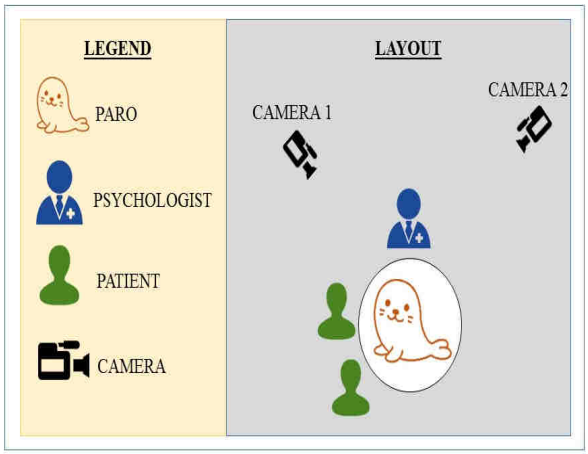

Figure 2 Proposed room layout for the experiment

and understanding to join the session and followed by Psychological screening which includes but not limited to DASS, BDI (Beck), BAI (Beck) and suicide screening. Next stage also involves setting up of the room at the rehabilitation center. The researchers also will consult and work together with the psychologist to conduct the session in the best way to benefit the patients.

2.2.2 Therapy Session

At this stage, therapeutic animal robot PARO will be introduced to a group of patient which consist of two participants. The aim session is to give a chance for participant familiar and interact directly with therapeutic animal robot PARO. The session will conduct in a conducive room with a psychologist, two patient and PARO, and two cameras to record the session. The first camera will be focusing on PARO itself, and the second camera with focus on the whole room. The preliminary actions that the psychologist need to demonstrate are:

a. Switch ON PARO at the tail
b. Hold PARO with both hands
c. Greet PARO with its name
d. Pet PARO's head
e. Pet PARO's body
f. Hold PARO hand starting form right to left
g. Hug PARO

The session continues with psychologist placing PARO on the table with patient. The patient will be encouraged to interact with PARO by psychologist in addition to topics of conversation throughout the session.

2.3 Data collection and Analysis

The interaction data will be in the form of:

a. Observation- From video records the patient-robot interaction throughout the sessions via a camera.
b. Time gathering- Compare total sleeping time of patient compare before and after session.
c. Stress leveling- By using stress meter device to measure stress level of patient before and after session.

3. RESULTS AND DISCUSSIONS

Three evaluation methods will be conducted. The first one is through observation via recorded videos. Observations are made based on the patient's body language and the patient's expression toward PARO. Based on the previous study [4], it is expected that the patients will show positive responses during the short interaction. The patients are also expected to initiate and communicate with the robot. Their facial expressions and eye-contact with the robot will show whether the patient had enjoyed the short interaction. The second method using sleeping time as accumulation data. The total time taken for patient to sleep will be evaluate. The time will be recorded for patient before engaging the therapy session and will be taken again the day after that in order to compare the improvement of sleeping time. The final method conducted by measuring the level of patient stress by using stress meter device. The patient will hold the device in their hand before starting the session with the robot to take the reading, and will be taken again after the session is finished.

4. CONCLUSIONS

The study expects that patients diagnosed or identified with symptoms of MDD could reduce their symptoms gradually until it is in remission, leading them being more interactive and socialize. From this finding, it is expected that this therapy session using therapeutic animal robot able to implement the epigenetic architecture model (ERA) involving people with MDD, psychologist and caregiver during rehabilitation period.

ACKNOWLEDGEMENT

The authors are grateful the Ministry of Higher Education Malaysia [FRGS/1/2016/SKK06/FKP-AMC/F00321], Universiti Teknikal Malaysia Melaka and SOCSO Rehabilitation Center Melaka for their support.

REFERENCES

[1] Y. Kawaguchi, K. Wada, M. Okamoto, T. Tsujii, T. Shibata and K. Sakatani, "Investigation of brain activity during interaction with seal robot by fNIRS," *RO-MAN, IEEE*, pp. 308-313, 2011.

[2] S.Y. Okita, "Self-other's perspective taking: the use of therapeutic robot companions as social agents for reducing pain and anxiety in pediatric patients," *Cyberpsychology, behavior and social networking*, vol. 16, no. 6, pp. 1-6, 2013.

[3] J. Pipitpukdee and W. Phantachat, "The study of the pet robot therapy in Thai autistic children," *Proceedings of the 5th International Conference on Rehabilitation Engineering & Assistive Technology 2011*, 2011, p. 43.

[4] S.M. Rabbitt, A.E. Kazdin and B. Scassellati, "Integrating socially assistive robotics into mental healthcare interventions: Applications and recommendations for expanded use," *Clinical psychology review*, vol. 35C, pp. 35–46, 2015.

Proceedings of Innovative Research and Industrial Dialogue'16, pp. 119-120 (May 2017)

Implementation of RFID on Reconfigurable Conveyor System

M.S. Osman, A.A.A. Rahman*, N.R. Mohamad, N.Z. Noridan

Integrated Manufacturing System (I'Ms) Group, Advanced Manufacturing System,
Universiti Teknikal Malaysia Melaka, Hang Tuah Jaya, 76100 Durian Tunggal, Melaka, Malaysia.

Email: azrulazwan@utem.edu.my

Keywords: RFID; Re-configurable Conveyor; Serial Communication

ABSTRACT – Implementation of RFID in reconfigurable conveyor is a monitoring improvement in manufacturing system. This study introduces the RFID system in reconfigurable conveyor by implementing tags on the pallets and on the conveyor module. A program interface will communicate with RFID module via serial communication to read the tags on the pallet while it moves through reconfigurable conveyor. The RFID module is attach on the reconfigurable conveyor module near the conveyor railway. the program interface also can show the configuration of the reconfigurable conveyor. For an improvement, database will be included in the system to store more information of RFID tags.

1. INTRODUCTION

RFID (Radio Frequency Identification System) is an identification tools that been used in matric card, credit or debit card and books in library. Moreover, Shoungho and Tomohiro found that RFID can be used to prevent collision accident with heavy equipment [1]. The purpose of this paper is to introduce RFID system in re-configurable conveyor system. Based on previous study, there are several benefits of RFID system being used in conveyor system. Firstly, implementation of RFID on conveyor system provide more transparent information on the material transferred. Besides that, RFID system simplify the stock count procedure and improving its accuracy. Furthermore, its can track the real-time and availability of the material on the conveyor system [2].

RFID tags can be implement at the pallet and on the module of reconfigurable conveyor. A reconfigurable conveyor system can change configuration easily and has conveyor module. Currently there are four conveyor configuration can be made in this study. The configurations are straight line, L-shaped, U-shaped and closed loop configuration. Different conveyor configuration used different arrangement of conveyor module. So the RFID tags can be attached on the reconfigurable conveyor module to determine the configuration. On the other hand, RFID tags can be place on the pallet so it can be monitor from software. The rest of the paper is organized as follows. In section 2, a brief overview of the work flow and component of RFID. The in section 3, result and discussion on the RFID program interface, serial communication and tags implementation. Finally, conclusion is drawn.

2. METHODOLOGY

Figure 1 shows the flowchart of the project. Based on Figure 1, preliminary study was conducted by referring from previous study on reconfigurable conveyor and RFID system. After that, the interface of the program is made based on the required information such as textbox to show the RFID tags and requirement of the user. Next, serial communication between RFID module and PC port was made. RFID module then programmed to read the RFID tags and lastly the RFID module is integrated on the reconfigurable conveyor.

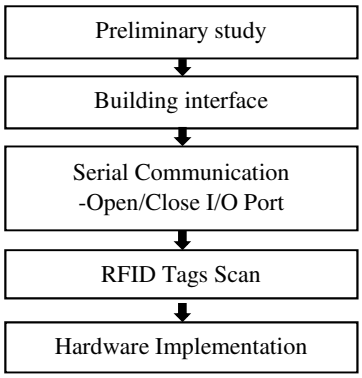

Figure 1 Flowchart

2.1 Components of RFID

RFID system is defined as physical and information based representation of an item which possesses a unique identification, capable of communicating effectively with its environment and can retain or store data about itself [3]. The component of RFID module used in this project is RFID reader/writer and passive RFID tags. RFID used in this project is APSX RW-210. The RFID reader has an onboard antenna with dimension of 114mm x 69mm x 6.4mm. The module can write or read up to 7cm with 24 mm circular labels tags.

Visual basic programming language is used in this project to create the interface program. Serial communication is used between visual basic and RFID module via RS232 cable. C100 module is used to convert from TTL readers to RS232. An adapter from RS232 to USB is used to changes from RS232 port to USB port.

3. RESULTS AND DISCUSSION

The implementation of RFID system on the reconfigurable conveyor can show the real time position of pallet and determine the configuration of reconfigurable conveyor. Figure 2 illustrates the concept of identification

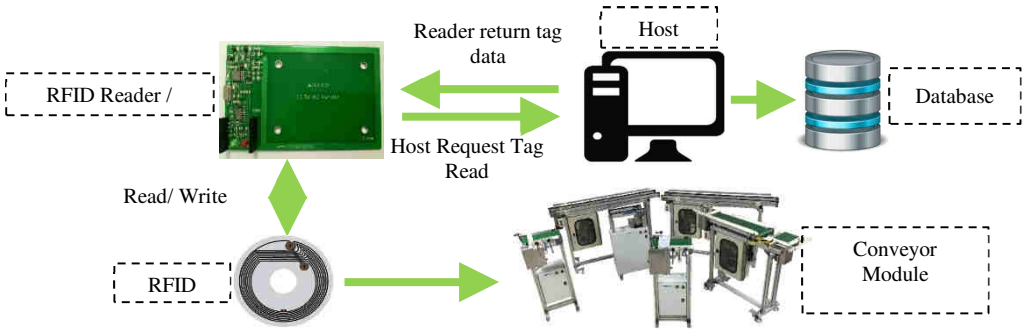

Figure 2 The concept of an identification system using RFID for reconfigurable conveyor

system using RFID on the reconfigurable conveyor. RFID tags is attached on the conveyor module or pallet. RFID reader or writer will scan on the RFID tags through serial communication. The host then will show the information on the tags scanned using the interface program. The information on the tags can be store in the database.

The interface program is create using visual basic language programming. Figure 3 shows the example of interface of the RFID program. The interface consists of three group. The first group is the port group. In port group there are open port button, close port button and list box which consist of connected port. On serial port, the default setting given was 9600 baud rate, data bits = 8, none parity, and stop bits is one. Com port need to be open before scanning else the RFID module is not communicated with the interface program. Available port can be select from the list box in port group.

The port that connected the RFID module can be checked on device manager under I/O ports. The open port button will be disabled as the port is already open.

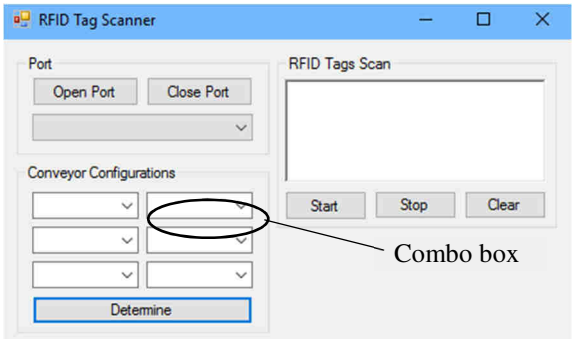

Figure 3 RFID Scanner Interface

The second group is RFID scan tags group. This group consists of three button which are start, stop and clear. Text box also included in the group to show the RFID tags ID. Start button is used for start the reading RFID tags loop. Stop button is used to stop the scanning tags loop and clear button is for clear the textbox. The textbox will continuously scan RFID tags and showed the RFID tags ID on every loop else the nothing will appear in the textbox which mean there are no tags scanned. The delay time for every loop is 250ms.

The third group is made to determine conveyor configuration. There are six combo boxes for each conveyor module. Conveyor module that scanned will be on the combo box. The conveyor configuration can be determined from the conveyor module that will be used. A message box will show the conveyor configuration. In the hardware implementation, RFID tags is implement on the pallet of reconfigurable conveyor. The tags are attach under pallets. Every pallet will have one RFID tags attach on it. A reader will be place near the pallet railway. The RFID reader or writer will be place approximately less than 7cm vertically from the pallet railway.

4. CONCLUSIONS

In conclusion, the RFID module can communicate with interface program via serial communication. The RFID tags reading is still in work progress. The interface program will be changed according to the information required by user. Database is an improvement to the project as to save the tags information on the pallet and configuration of the reconfigurable conveyor system.

ACKNOWLEDGEMENT

The authors would like to acknowledge the financial and administrative support from the Minister of Education (MOE), Malaysia and Universiti Teknikal Malaysia Melaka under the FRGS/1/2014/TK01/FKP/03/F00229 Research grant Project entitles “A novel concept of reconfigurable material handling systems to support changeability in manufacturing”.

REFERENCES

[1] S. Chae and T. Yoshida, “Application of RFID technology to prevention of collision accident with heavy equipment,” *25th International Symposium on Automation and Robotics in Construction*, vol. 19, no. 3, pp. 368-374, 2010.

[2] E.W.T. Ngai, F.F.C. Suk and S.Y.Y. Lo, “Development of an RFID-based sushi management system: The case of a conveyor-belt sushi restaurant,” *International Journal of Production Economics,* vol. 112, no. 2, pp. 630-645, 2008.

[3] V. Vlad, A. Graur, C.E. Turcu, C. Popa, “Enhancing the flexibility of manufacturing systems using RFID technology”, *International Conference on Advanced Information Networking and Applications Workshop,* 2009, pp. 630-635.